Fracture Mechanics of Concrete and Concrete Structures - Recent Advances in Fracture Mechanics of Concrete - B. H. Oh, et al.(eds)
 ISBN 978-89-5708-180-8

Discrete element model of concrete under high confining pressure

V.T. Tran, F.V. Donzé & P. Marin
Laboratoire "Sols, Solides, Structures et Risques" (3S-R), Université Joseph Fourier, Grenoble Université-CNRS, BP53, 38041 Grenoble cedex 9, France

ABSTRACT: A numerical model based on a three dimensional Discrete Element Method (DEM) has been used to study the behavior of cohesive granular geomaterials such as concrete under a high confining pressure (up to 650 MPa). At this range of pressures, irreversible compaction of the material occurs and needs to be considered. Within the discontinuous nature of the model, a local constitutive law has been developed to reproduce this phenomenon quantitatively. The computational implementation has been carried out in the Discrete Element and open source code YADE (Kozicki & Donze 2008)

1 INTRODUCTION

Concrete is used for sensitive infrastructures like nuclear power reactors. However, concrete exhibits an intrinsically complex behavior (Gabet et al. 2006) under extreme loading, such as explosions or ballistics impacts (Shiu et al. 2008) which is difficult to reproduce experimentally. To predict its response under dynamic loading, its experimental static behavior under very high confinement must first be characterized. Since it will generate different damage modes which strongly depend on the stress state and the loading path, brittle damage and irreversible strain such as compaction must be well understood.

Extensive micro-cracking and macro-cracking are difficult to characterize in terms of a continuum formulation, this is why it has been chosen to use a discrete model (Cundall & Hart 1992, Donzé & Magnier 1995) to represent the material as an assemblage of independent elements, interacting with one another. It directly takes into consideration the physical mechanisms and the influence of the concrete aggregate structure, offering an interesting alternative tool to reproduce a fracturing process in concrete.

The purpose of the present study is therefore to set up the formulation of the local constitutive laws for a 3D discrete element model in order to represent the behavior of concrete at high confining pressure. Based on the simulation of experimental tests (Gabet et al. 2008, Vu et al. 2009) performed previously on a low-strength plain concrete, (using the large capacity triaxial "GIGA" press, stress levels above 1 GPa with homogeneous, static and well controlled loading paths could be reached), the numerical model was first calibrated from both, tri-axial tests carried out at low confining pressure and hydrostatic test. Once the model's parameters have been obtained, the model was used to predict the response of a concrete sample for tri-axial tests at different levels of confinement (Tran et al. 2009).

2 DISCRETE ELEMENT MODEL

There are different Discrete Element Methods applied in the Geotechnical field, and we will use in this work the classical Discrete (or Distinct) Element Method (DEM) formulation pioneered by Cundall & Strack (1979). Basically, the algorithm involves two steps. In the first one, interaction forces are computed when elements slightly interpenetrate each other: this force-displacement formulation is often referred to as a Smooth contact method or also as the Force-Displacement method. In the second step, Newton second law is used to determine, for each Discrete Element (DE), the resulting acceleration, which is then time integrated to find the new element positions. This process is repeated until the simulation is finished. This simultaneous numerical solution of the system is also known as the Molecular Dynamics (MD) formalism.

For small deformations, cohesive frictional geomaterials exhibit a linear elastic response. To reproduce this behavior, linear elastic interaction forces between the discrete elements are sufficient and lead to small simulation times. In the present model, the initial elastic interaction force, which represents the action of element a on element b, does not only involve elements in contact, but elements which are also separated by a distance smaller than an interaction radius controlled by a ratio γ defined by,

$$\gamma(R_a + R_b) \geq D_{ab} \qquad (1)$$

where D_{ab} is the distance between the centroids of elements a and b; R_a and R_b are the radii of elements a and b; and $\gamma \geq 1$.

This is an important difference from classical discrete element methods which use spherical elements where only contact interactions are considered (γ = 1). γ was chosen so that the average number of interactions per DE equals 12. By setting such a ratio, the macroscopic Young's modulus which depends on the local stiffnesses is controlled more easily (Hentz et al. 2004a, Rousseau et al. 2008). However, this mid-range interaction is limited to nearest neighbors.

The interaction force vector **F** which represents the action of DE a on DE b may be decomposed into a normal force vector $\mathbf{F}_n$ and a shear force vector $\mathbf{F}_s$ which may be classically linked to relative normal and incremental shear displacements respectively, through the stiffnesses, K_n and K_{n2} in the normal direction and K_s in the tangential direction (Hart et al. 1988).

The normal interaction force can be calculated through the updated local constitutive law, which is shown in Figure 1, and can be split into two parts, the compressive and the tensile components. In the compressive part, we propose a more complete formulation of F_n in order to take into account the compaction process which occurs at a lower scale than the discretization size of the model. In this formulation, the concrete's response is first linear (section AB in Fig. 1) and the normal interaction force is given by,

$$F_n = K_n(D_{eq} - D_{ab}) \tag{2}$$

where F_n is the normal interaction force, D_{eq} is the initial distance between two DE a and DE b respectively.

Then, when the interaction's deformation reaches an elastic deformation limit $\varepsilon_{\max}$ which is related to the interaction distance D_1, a hardening-damage response is considered (section BC in Fig. 1). At this step of the interaction, the normal interaction force is characterized by a nonlinear stiffness K_{n2}, which is an exponential function of the deformation and controlled by three parameters ζ_1, ζ_2 and ζ_3. This stiffness is expressed as,

$$K_{n2} = K_n\left[\zeta_1 * \left(e^{\zeta_2(\varepsilon - \varepsilon_{\max})}\right) + \zeta_3\right] \tag{3}$$

where maximum elastic deformation is defined by,

$$\varepsilon_{\max} = \frac{D_{eq} - D_1}{D_{eq}} \tag{4}$$

So, the complete normal interaction force is expressed as,

$$F_n = K_n(D_{eq} - D_1) + K_{n2}(D_1 - D_{ab}) \tag{5}$$

In the tensile part, the normal interaction force can also be computed with Equation 2. However, the stiffness may be modified by a softening factor ζ while the softening behavior occurs after the normal force has reached its maximum value, $F_{n,\max}$, which is calculated by Equation 10. Therefore, the normal force is now calculated such that,

$$F_n = \left(D_{ab} - D_{rupture}\right)\frac{K_n}{\zeta} \tag{6}$$

when the rupture occurs ($D_{ab} > D_{rupture}$), the interaction forces are set to zero.

The shear force vector $\mathbf{F}_s$ is calculated by updating its orientation which depends on the orientation of the direction passing through the two centroids of the interacting DE, and by adding the increment $\Delta\mathbf{F}_s$ (Hart et al. 1988), which is defined by

$$\Delta\mathbf{F}_s = K_s\Delta\mathbf{U}_s \tag{7}$$

where $\Delta\mathbf{U}_s$ is the increment shear displacement vector between the locations of the interacting points of the two elements over a timestep Δt.

Note that the stiffnesses used here depend on the macroscopic elastic property and the size of the elements and can be expressed as,

$$K_n = \alpha * E * R_{avg} \tag{8}$$

$$K_s = \beta * K_n \tag{9}$$

where α and β are dimensionless coefficients; E is Young's modulus, which is set here using the value obtained by a compressive experiment test (Gabet et al. 2008); and R_{avg} is the average radius of the two interacting elements.

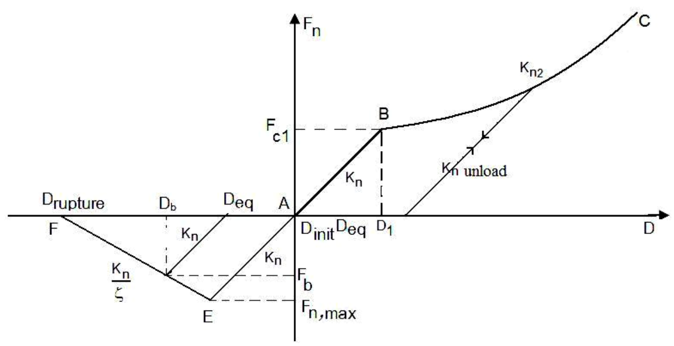

Figure 1. Summarizes the constitutive law.

To model the nonlinear behavior of the concrete material, a modified Mohr-Coulomb model has been used (Fig. 2). For a given interaction, the maximum normal interaction force $F_{n,\max}$ is defined as a function of tensile strength T. The maximum shear interaction force $F_{s,\max}$ is characterized by the normal force F_n, the cohesion C, the contact frictional angle Φ_c and the internal frictional angle Φ_i. Therefore, the maximum normal force can be defined as,

$$F_{n,\max} = -TA_{\text{int}} \tag{10}$$

where $A_{\text{int}} = \pi(\min(R_a, R_b))^2$ is defined as the interacting surface.

The maximum shear force is calculated for a "link" interaction, such that
If $F_n \tan\Phi_i < (\lambda - 1)\, C\, A_{int}$:

$$F_{s,\max} = F_n \tan\Phi_i + CA_{\text{int}} \tag{11}$$

else

$$F_{s,\max} = \lambda CA_{\text{int}} \tag{12}$$

where λ is a dimensionless coefficient, which has been added to control the sliding threshold of the link interaction.

When the new contacts appear during the simulation, their maximum shear force will only be frictional,

$$F_{s,\max} = F_n \tan\Phi_c \tag{13}$$

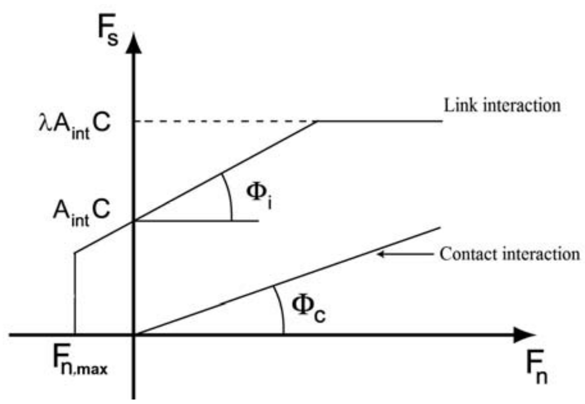

Figure 2. Rupture criterion used in the model.

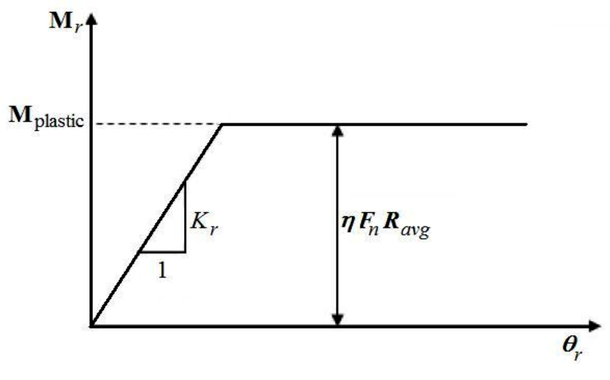

Figure 3. Rolling moment law considered between interacting DE.

To reproduce quantitatively the behavior of a granular material when spherical discrete elements are used, the interaction between DE must transmit a moment (Alonso-Marroquin et al. 2006, Plassiard et al. 2009) which controls the rolling occurring during shear displacement. Doing so, the sliding process increases and the resulting friction angle can reach values corresponding to those measured for concrete materials. This moment transferred between two elements in interaction can be written as,

$$M_{elast} = \sum \theta_r K_r \tag{14}$$

where θ_r is the relative rotation angle and K_r is the rotational stiffness.

An elastic limit is introduced and when it is reached, the plastic moment defined by,

$$M_{plast} = \eta F_n R_{avg} \tag{15}$$

will take place (Fig. 3). Here, η is a dimensionless factor used for the plastic moment and R_{avg} is the average radius of two interacting DE. Note that the expression of the local parameters includes the characteristic size of the DE. The macroscopic mechanical properties therefore tend to be independent of the DE's size.

3 NUMERICAL SIMULATIONS

The numerical model has been set up to simulate the experimental tests carried out by Gabet (Gabet et al. 2008). For this purpose, the local parameters of model were first identified using uniaxial compressive – tensile tests, hydrostatic tests at 650 MPa and the triaxial test carried out at 50 MPa. Once calibrated, the model made of polysized Discrete Elements, to ensure an isotropic behavior, will be used to predict the concrete sample's responses for the other confining pressures.

3.1 *Numerical sample preparation and monitoring*

The generated numerical sample is a parallelepiped and not a cylinder as in the experiments. This has been chosen to potentially investigate anisotropic loadings, but one could expect that the geometry has a negligible effect on the results (Haimson & Chang 2000). The number of DE in the numerical sample is about 10000 and the resulting sample measures 0.07 m×0.14 m×0.07m.. The positions and diameters of the DE have been generated randomly.

A true numerical triaxial test is done using the following protocol. First, the numerical sample is subjected to a hydrostatic confining pressure up to a pressure value p, by moving surrounding plates (Fig.

4). Once this pressure value is reached, the top and bottom plates are moved vertically as loading platens, using a force-controlled condition. During the loading of the test, the displacement of the lateral plates are controlled to maintain a constant confining pressure p. Note that, these numerical tests are carried out with frictionless lateral plates, similar to the experimental condition tests (Gabet et al. 2008), in which a confining fluid is used. To be as close as possible to the experimental tests, a small friction value is considered between the sample and the loading platens in the numerical case. The axial stress is computed by dividing the total axial force applied to the top plate to the sample by its surface and the deformations are computed via the movement of plates.

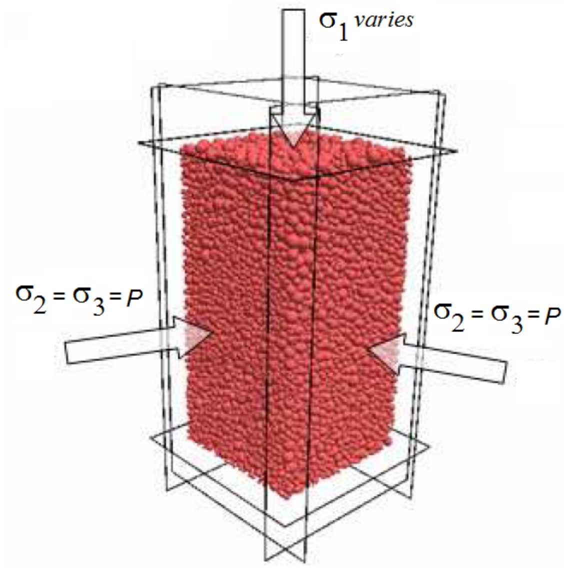

Figure 4. Configuration of triaxial test.

3.2 *Calibration*

The calibration of the model parameters is a necessary step to simulate quantitatively the behavior of a real geomaterial. It is conveniently done by comparing real and simulated reference tests. These comparisons will lead to set up the model's parameters, such as the tensile strength T, the cohesion C, the softening factor ζ, the internal friction angles Φ_i and Φ_c, the stiffnesses' coefficients (α, β, ζ_1, ζ_2 and ζ_3), the maximum elastic deformation $\varepsilon_{\max}$ and the coefficient of maximum shear force λ. The interaction's range γ has been fixed by the geometry of the numerical sample and its value is 1.37. The identification procedure (which has been already developed in similar in previous works (Hentz et al. 2004b, Rousseau et al. 2008)) is through a group of reference tests which include, a uniaxial compression-traction test, a hydrostatic test at 650MPa and a triaxial 50MPa test.

The uniaxial compression-traction tests have been used to calibrate the local parameters α, β, C, ζ, T, Φ_i and Φ_c. First of all, the linear stiffnesses' coefficients α and β were varied to match Young's modulus and Poisson's ratio of the concrete material while all other parameters of the test were kept constant with a sufficiently high value to respect a purely elastic response of the model. The uniaxial tensile test was used to evaluate the local tensile strength T and the softening coefficient ζ. Then, the compressive test was used to evaluate the values of the cohesion C, the friction angles Φ_i and Φ_c. These values were chosen according to the macroscopic values, such as the compressive strength σ_c and the tensile strength σ_t. Doing so, the numerical and experimental results for the tensile and compressive tests show quite a good agreement (see Fig. 5, where the axial stress σ_1 versus the axial strain ε_1 and the lateral strain ε_2 are plotted).

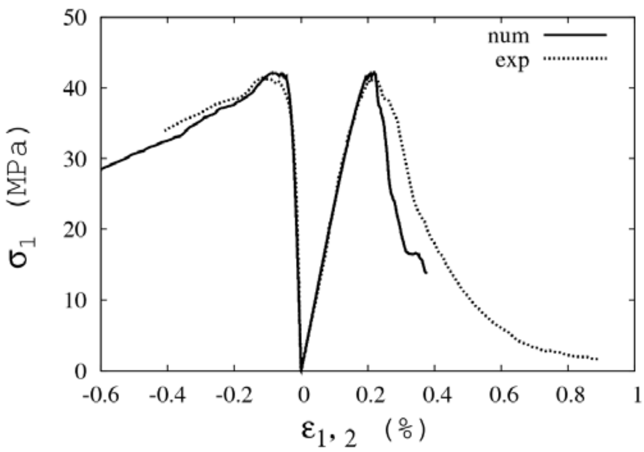

Figure 5. Stress-strain curves for uniaxial compressive test. Solid and dotted lines correspond to the numerical and experimental results respectively.

The uniaxial compression test is not sufficient to calibrate the full irreversible response of the model, which is also characterized by the three hardening stiffness ratios ζ_1, ζ_2, ζ_3 and the maximum elastic deformation $\varepsilon_{\max}$. This is why an experimental hydrostatic test performed with a confining pressure reaching 650MPa was used. With this hydrostatic test, it was possible to obtain information on the compaction process of the concrete material and to evaluate the contribution of this phenomenon.

The full triaxial 50MPa test was used to finish the calibration process by fixing the value of the rupture criterion coefficient λ. This parameter controls the maximum shear force. When the lateral deformation decreases, a transition contraction-dilatancy is observed in the experiments (Fig. 6). This volumetric transition is well reproduced by the model when choosing the right value for λ.

Thus, the full elastic-hardening-damage law of the numerical model can reproduce quantitatively the experimental triaxial compressive test carried out by Gabet (Gabet et al. 2008). The local parameters of the model have been calibrated and their values are given in Table 1.

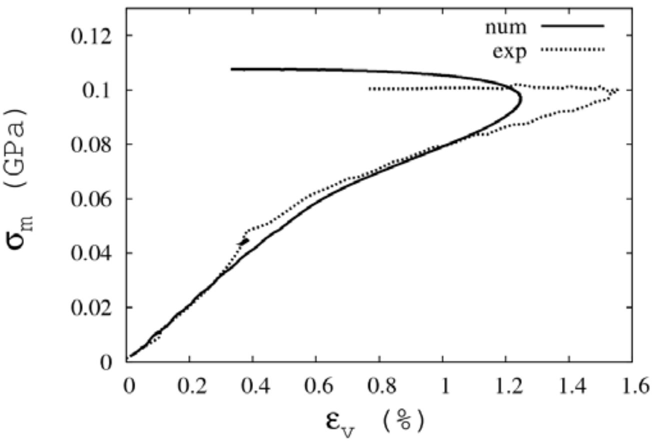

Figure 6. Mean stress-volumetric strain curves at 50MPa confining pressure. Solid and dotted lines correspond to the numerical and experimental results respectively.

Table 1. Local parameter values of the numerical model.

Parameters	Values
Coefficient α	1
Coefficient β	0.25
ε_{max} (%)	0.2
Tensile limit (MPa)	9
Cohesion C (MPa)	4
Softening ζ	5
Frictional angles Φ_i and Φ_c (°)	30
Coefficient ζ_1	0.2
Coefficient ζ_2	16
Coefficient ζ_3	0.275
Coefficient λ	5

3.3 *Prediction for the other confining pressure*

The model parameters have been calibrated using uniaxial compressive-tensile, hydrostatic at 650MPa and triaxial at 50MPa tests. Without changing the values of these parameters, the numerical model is now used to simulate triaxial tests at other confining pressures. Four triaxial tests have been simulated for the following confining pressures: 100 MPa, 200 MPa, 500 MPa and 650 MPa. They are compared with data also available in the experimental campaign. For all theses cases, the same initial numerical parallelepiped sample has been used. Both, experimental and numerical results are presented with lateral-axial strain/axial stress components and volumetric curves.

3.3.1 *Strain-stress response of triaxial tests*

The results indicate that in the hydrostatic phase, the numerical results are very close to the experimental measurements.

In the differential-stress phase, the simulated results are overall comparable with the experimental ones. Experimentally, for the 100MPa test, a stagnation of the axial pressure is observed, without reaching a peak as is the case in the 50MPa test. Then, for the 500MPa and 650MPa tests, the stiffness curves gradually decrease without changing slope. All the numerical curves show a stress peak and before it occurs, a decrease of the stiffness is observed in both the model and the experiments. The numerical and the experimental results differ in that the axial stress peaks are reached earlier in the numerical model than in the experiment. When adding friction on the lateral plates in the numerical sample, this discrepancy tends to vanish. However, by doing so the elastic deformation is no longer homogeneous in the numerical sample. Thus, a clear explanation could not be obtained from the model, despite a large parametric study.

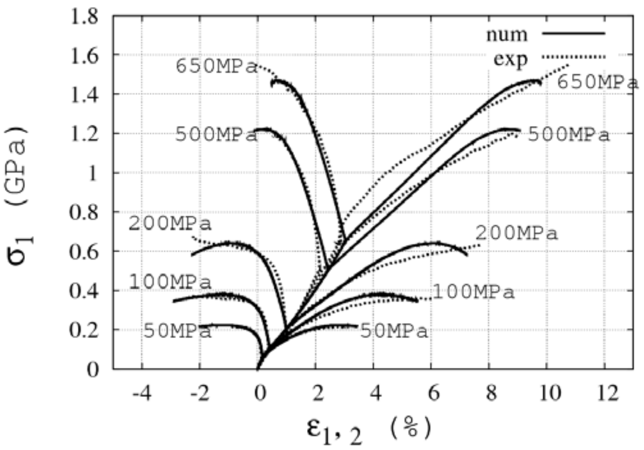

Figure 7. Stress-strain curves for 50MPa, 100MPa, 200MPa, 500MP and 650MPa (c) confining pressures. Solid and dotted lines correspond to the numerical and experimental results respectively.

3.3.2 *Volumetric behavior and limit state*

As expected, the numerical and experimental volumetric deformations on the hydrostatic phase seem to fit very well (see Fig. 8). However, when the contraction-dilatation transition occurs at the same mean stress value, the amplitudes of the maximum contraction of the numerical volumetric curves are lower than the experimental ones. This result is directly linked to the observations made on the stress-strain curve, and the conclusions are similar. Note that in the 500MPa experimental test, the results do not show a contraction-dilatancy transition because this test has been prematurely stopped.

Another way to deal with the contraction-dilatancy transition (also called the limit state), is to represent it in the (σ_m, q) stress space (see Fig. 9). Here again, the experimental and numerical results are in a very good agreement. Thus, it can be concluded that the numerical model can reproduce macroscopic key properties such as the volumetric strain of concrete during the hydrostatic phase and the contraction-dilatancy transition.

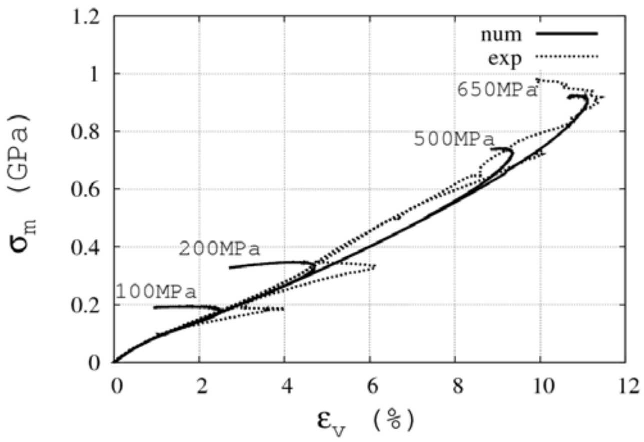

Figure 8. Mean stress-volumetric strain curves for the 100MPa, 200MPa, 500MPa and 650MPa confining pressures. Solid and dotted lines correspond to the numerical and experimental results respectively.

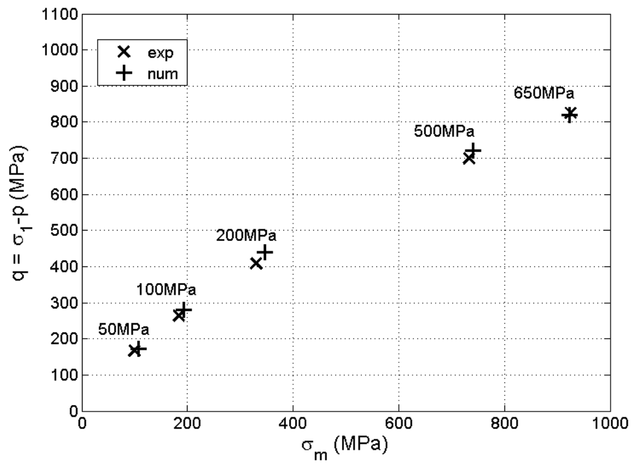

Figure 9. Limit state points, defined as contraction-dilatancy transition on the volumetric behavior curves for the experimental and numerical tests, are represented in the (σ_m, q) stress space.

4 CONCLUSION

A Discrete Element Model using a local elastic-hardening-damage constitutive law has been formulated to reproduce the behavior of concrete at high confining pressures. Regarding the reduced set of experimental data, a calibration step has been done prior to using the model for predictive simulations. The results show that the experimental stress-strain and volumetric curves were quantitatively well reproduced. The compaction process results from a coupling between an elastic behavior and two simultaneous irreversible phenomena which are, the collapse of the porosity of the sample and the structural de-cohesion of the cement matrix (Gabet et al. 2008). When the confining pressure is high, the rearrangement of the DEs within the numerical model is no longer possible, since the DE cannot be deformed and only overlapping is authorized. Thus, the only way to simulate the compaction process is to control how the overlapping will evolve and this is done by adding the non-linear hardening step to the compressible part of the interaction forces. The key point is that when using a description of the medium, by simply adding this normal interaction force type, it is possible to get a good macroscopic description (i.e. stress-strain or volumetric curves).

REFERENCES

Alonso-Marroquin, F., Vardoulaskis, I., Herrmann, H.J., Weatherley, D. & Mora, P. 2006. Effect of rolling on dissipation in fault gouges. *Physical Review E*, 74 3a.

Cundall, P.A. & Hart, R.D. 1992. Numerical modeling of discontinue. *Engineering Computations* (6): 101-113.

Cundall, P.A. & Strack, O.D. 1979. A discrete numerical model for granular assemblies. *Geotechnique* 29: 47-65.

Donzé, F.V. & Magnier, S.A. 1995. Formulation of the three-dimensional numerical model of brittle behavior. *Geophysical Journal International* 122: 790-802.

Gabet, T., Vu, X.H., Malecot, Y. & Daudeville, L. 2006. A new experimental technique for the analysis of concrete under high triaxial loading. *Journal de Physique IV* 134: 635-640.

Gabet, T., Malecot, Y. & Daudeville, L. 2008. Triaxial behavior of concrete under high stress: Influence of the loading path on compaction and limit states. *Cement and Concrete Research* 38: 403-412.

Haimson, B. C., & C. Chang, 2000. A new true triaxial cell for testing mechanical properties of rock, and its use to determine rock strength and deformability of westerly granite, *Int. J. Rock Mech. Min. Sci.*, 37:285– 296.

Hart, R.D., Cundall, P.A. & Lemos, J. 1988. Formulation of a three-dimensional distinct element model. II: Mechanical calculations for motion and interaction of a system composed of many polyhedral blocks. *Int. J. Rock Mech. Min. Sci. Geomech. Abstr.* 25: 117-125.

Hentz, S., Daudeville, L. & Donzé, F.V. 2004a. Discrete element modelling of concrete submitted to dynamic loading at high strain rate. *Computers and Structures* 82(29-30): 2509-2524.

Hentz, S., Daudeville, L. & Donzé, F.V. 2004b. Identification and validation of a discrete element model for concrete. *J. Eng. Mech*. 130(6): 709-719.

Kozicki, J. & F.V. Donzé, 2008, Applying an open--source software for numerical simulations using finite element or discrete modelling methods. Computer Methods in Applied Mechanics and Engineering, 197(49-50), pp. 4429-4443.

Plassiard, J.P., Belheine, N. & Donzé, F.V. 2009. A spherical discrete element model: calibration procedure and incremental response. *Granular Matter*, DOI: 10.1007/s10035-009-0130-x, online.

Rousseau, J., Frangin, E., Marin, P. & Daudeville, L. 2008. Damage prediction in the vicinity of an impact on concrete structure: a combined FEM/DEM approach. *Computers and Concrete* 5(4): 343-358.

Shiu, W., Donzé, F.V. & Daudeville, L. 2008. Compaction process in concrete during missile impact: a DEM analysis. *Computers and Concrete* 5(4): 329-342.

Tran, V.T, Marin, P. & Donzé, F.V. 2009. Modeling cohesive granular geomaterials under high confing pressure with a discrete element method. *Journal of the Mechanics and Physics of Solids*, submitted.

Vu, X.H., Malecot, Y., Daudeville, L. & Buzaud, E. 2009. Experimental analysis of concrete behavior under high confinement: Effect of the saturation ratio. *International Journal of Solids and Structures* 46: 1105-1120.